Measurement 46 (2013) 871–880

Contents lists available at SciVerse ScienceDirect

Measurement

journal homepage: www.elsevier.com/locate/measurement

Emissivity estimation for high temperature radiation pyrometry on Ti–6Al–4V

Petter Hagqvist *, Fredrik Sikström, Anna-Karin Christiansson

University West, Department of Engineering Science, SE-46186 Trollhättan, Sweden

ARTICLE INFO

Article history:
Received 29 February 2012
Received in revised form 29 June 2012
Accepted 9 October 2012
Available online 12 November 2012

Keywords:
Ti–6Al–4V
Temperature
Emissivity
Radiation pyrometer
Laser metal deposition
Calibration

ABSTRACT

The paper demonstrates a versatile procedure suitable for industrial implementation of temperature measurement on a hot titanium alloy. The driving force has been the need for an accurate temperature measurement during additive manufacturing using laser welding technology where Ti–6Al–4V-wire is melted. The challenges consider both industrial constraints and the varying emissivity of the surface. Measurements makes use of a narrow bandwidth spot radiation pyrometer and a calibration procedure for estimation of the surface temperature through spectral emissivity estimation. The theoretical results are validated through experiments. A number of difficulties in radiation temperature measurements for metals with varying surface properties are discussed; especially the case of surface oxidation. The uncertainty in temperature reading due to the uncertainty in the emissivity estimate is established along with a model that qualitatively describes surface oxidation. The procedure is expected to be useful for several manufacturing applications where it is important to control high temperatures.

1. Introduction

This paper describes the emissivity estimation of titanium alloy Ti–6Al–4V to be used in narrow wavelength radiation pyrometry during melting processing. The motivation for the study is the need for temperature measurements in laser metal deposition (LMD) [1]. One of the most prominent sources of uncertainty in radiation pyrometry is the estimation of the measurand surface emissivity. This is especially true in case of shiny metals where the emissivity is far from unity and the level of uncertainty is more critical [2]. An accurate temperature measurement therefore requires knowledge of the object's emissivity. Different methods of correction to reduce the influence of the emissivity are described in the literature, e.g. [3]. However there is no general approach that guarantees a limit in the uncertainty in temperature measurements for a certain material during specific measuring conditions. Generally there are no data on temperature and wavelength dependency of emissivity of commercial alloys. Neither does available data take into account the surface oxidation, which is an inevitable consequence when heating non-noble metals such as titanium in the presence of oxygen.

In addition to the applications within LMD and welding-like processes for both Ti–6Al–4V and other materials, non-contact temperature measurements are vital within processes such as heat treatment of metals, laser cutting and within the semiconductor, paper, food and asphalt industries [4]. For some of these applications, determination and estimation of emissivities are major challenges. Research within this field will therefore not only give substantial benefits for those industries but also open up new applications for non-contact thermometry where this technique is not an option today due to the problem of unknown and varying emissivities.

The titanium alloy Ti–6Al–4V is commonly used within aerospace applications and for other components with demands on high performance and low weight [5]. Fabricating these components through various melting

* Corresponding author. Tel.: +46 520223288.
E-mail address: petter.hagqvist@hv.se (P. Hagqvist).

0263-2241/$ - see front matter © 2012 Elsevier Ltd. All rights reserved.
http://dx.doi.org/10.1016/j.measurement.2012.10.019

processes has grown increasingly important along with raised demands on fuel efficiency within the aero-engine industry [6]. While employing melting processes such as LMD of Ti–6Al–4V a need has been identified of non-contacting temperature measurements [1,7,8]. Temperature information is important for on-line process control and monitoring in order to understand and optimise the process and to mitigate disturbances and perturbations [1]. It is also necessary for calibration and validation of LMD process models, typically finite element models, for predicting of material characteristics that are strongly dependent on the temperature history, e.g. microstructure modelling [7]. When predicting the bead geometry, through mass and heat flow modelling temperature is also critical for model calibration [8].

Due to the nature of LMD, where the geometry is built up during processing, contacting temperature measurement methods are not viable. Imaging or point measurement techniques are required to obtain spatially dependent temperature information in and around the melt pool. Due to the availability of focusing optics for radiation pyrometry, measurements with spots less than 1 mm in diameter for high spatial resolution are an option besides thermal cameras. Other non-contact temperature measurement methods previously used for LMD include photodiodes, either single diodes or several arranged in arrays [9–11]. Methods using photodiodes however give more limited information about local temperature in the object than what is possible with a focused radiation pyrometer or a thermal camera [11]. Thermal cameras however make data analysis harder since surface characteristics vary over the examined area. Further, they must be positioned close to the process since optical fibres cannot be used for transferring an image to the detector. Such positioning demands require space and possibly a cooling solution to protect the detector and sensitive electronics from the elevated temperature inside the process chamber. Also, there is a risk of camera optics focusing laser reflections, which might severely damage the detector. This risk is avoided when using a pyrometer together with a focusing optical head that do not allow stray reflections to hit the detector. As monitoring localised temperature with good spatial resolution is important for control and simulation purposes and infrared imaging cameras are deemed unpractical for the application, radiation pyrometry with focusing optics is the approach further investigated in this study.

2. Theory

Narrow wavelength range pyrometry is an important special case of radiation pyrometer methods. Its importance is due to the simplicity of the method and also due to its usefulness in industrial settings.

2.1. Narrow wavelength radiation pyrometry

In radiation pyrometry, the emitted energy of an object within certain regions of the electromagnetic spectrum, is measured quantitatively. A blackbody's radiance, which is the energy emitted at a certain wavelength λ_0, at the absolute temperature T_A, is given by Planck's law [12,13];

$$i_b(T_A,\lambda_0)=\frac{2\pi C_1}{\lambda_0^5(e^{C_2/(\lambda_0 T_A)}-1)}, \tag{1}$$

where $C_1 = 3.742\times10^8$ W μm m^{-2} and $C_2 = 1.439\times10^4$ μm K [13]. The integral of (1) over all wavelengths gives the intensity I_b of the blackbody radiation;

$$I_b(T_A)=\int_\lambda i_b(T_A,\lambda)d\lambda. \tag{2}$$

The radiation emitted from a physical object is not identical to that of an idealised blackbody, hence the concept of emissivity comes to play [13]. Spectral-directional emissivity, $\varepsilon(T_A,\lambda,\theta,\phi)$, is a surface property dependent not only on the surface's chemical composition but also on, the absolute temperature T_A, the wavelength λ, the incident inclination angle θ, and the azimuth angle ϕ. Spectral-directional emissivity is defined as the ratio of the radiance emitted by a physical body $i_p(T_A,\lambda,\theta,\phi)$ to that of an idealised blackbody of the same temperature [13];

$$\varepsilon(T_A,\lambda,\theta,\phi)=\frac{i_p(T_A,\lambda,\theta,\phi)}{i_b(T_A,\lambda)}. \tag{3}$$

The signal from a radiation pyrometer u is here modelled as the integrand of the product of the total received radiance i_{tot} and the spectral responsiveness of the pyrometer $k(\lambda)$. The function $k(\lambda)$ incorporates the transmission through the optical path in the sensor and the detector sensitivity. The received radiance i_{tot} consists of three parts, where the radiation $i_{p_{T_A}}$ emanates from the measurand at temperature T_A, the irradiation $i_{p_{T_W}}$ emanates from ambient objects at temperature T_W, and the irradiation $i_{p_{T_{atm}}}$ emanates from the intervening atmosphere with temperature T_{atm}. Hence the total received radiance is $i_{tot}=\varepsilon\tau i_{b_{T_A}}+\tau(1-\varepsilon)i_{p_{T_W}}+(1-\tau)i_{p_{T_{atm}}}$ where $\tau(\lambda)$ is the atmospheric transmission. Here the measurand is assumed to be opaque meaning that the transmission through it is zero and Kirchhoff's law of thermal radiation [13] from it reduces to the sum of emissivity ε and reflectance ρ only, $\varepsilon+\rho=1$. The signal from a radiation pyrometer thus becomes;

$$u=\iiint_{\lambda\theta\phi} k i_{tot}\,d\phi\,d\theta\,d\lambda. \tag{4}$$

It can be justified to introduce a number of assumptions. First, the viewing direction is assumed to be close enough to the normal in order for emissivity due to viewing direction variations to be assumed constant. This leads to that the dependency of the angles, θ and ϕ, is neglected [13]. The irradiations $i_{p_{T_W}}$ and $i_{p_{T_{atm}}}$ are also regarded as insignificant and neglected since $T_W \ll T_A$ and $T_{atm} \ll T_A$. The atmospheric transmission τ is assumed to be unity due to the absence of absorbing gases and fumes and also due to the short distance between the mesurand and the sensor (approximately 0.2 m). $k(\lambda)$ is assumed constant, $k(\lambda)\approx\kappa$, in the narrow wavelength interval $\lambda_r\in\left[\lambda_c\pm\frac{\Delta\lambda}{2}\right]$ where the pyrometer operates. With these assumptions

u/κ is reduced to an integral of $i_p(T_A,\lambda)$. Assuming an interval where $\Delta\lambda \to 0^+$ the following approximation is valid;

$$I_p(T_A,\lambda_r) = \int_{\lambda_r} \varepsilon(T_A,\lambda) i_b(T_A,\lambda) d\lambda \approx i_p(T_A,\lambda_c)\Delta\lambda. \quad (5)$$

The signal $u(T_A,\varepsilon)$ at λ_r is thus modelled as proportional to the product of the radiative intensity (5) and the constant κ;

$$u(T_A,\varepsilon) = \kappa i_p(T_A,\lambda_c)\Delta\lambda = \kappa\varepsilon(T_A,\lambda_c) i_b(T_A,\lambda_c)\Delta\lambda. \quad (6)$$

Here the emissivity dependency of λ is neglected due to the assumption that it is approximately constant in a sufficiently narrow wavelength region. Thus, if all the assumptions hold and by knowing κ, the pyrometer can be used to measure the temperature T_A with emissivity $\varepsilon(T_A)$ as the only tuning parameter.

2.2. Difficulties in spectral radiation pyrometry

In order to measure temperature one could either supply emissivity values to a narrow wavelength pyrometer or employ two or several wavelength regions [13]. If two or more wavelengths are used, commonly called multicolour pyrometry, the emissivity factor can be eliminated provided the ratio between emissivities in different spectral regions are known. However multicolour pyrometry requires that emissivity ratios are constant and do not change with temperature [13]. There are also methods for the emissivity alone, for example by heating a specimen in a vacuum chamber and using an FT-IR spectrometer as described by del Campo et al. [14]. Another method uses spectral information to simultaneously resolve both the emissivity and temperature, even without *a priori* modelling of emissivity [15].

In contrast to the latter method, Duvaut in his investigation of multispectral pyrometry methods [16,17], concludes that there is no automatic method to employ when using multispectral information, and that knowledge of suitable emissivity models for the material are required. He further mentions that multiwavelength methods however seem well adapted for measurements where temperature and emissivity change rapidly, provided good models are available.

In the book *Radiometric Temperature Measurements*, Zhang and Machin [2] advise that if no reliable model of spectral emissivity is available, a narrow wavelength radiation pyrometer (assumed to be wavelength independent in the narrow wavelength band λ_r) combined with a good emissivity estimation is the best choice. They argue that surfaces with wavelength independent emissivity, so called graybodies, are rare and that multiwavelength radiation pyrometry has distinct disadvantages compared to a narrow waveband radiation pyrometer if no *a priori* knowledge of emissivity is present. These disadvantages of multiwavelength methods include the fact that an increased number of channels lead to increased error propagation when measurement errors are present. Also, fitting a mathematical model to measurement data may lead to either over- or underfitting, if the model employed is unsuitable for describing the underlying phenomena [18].

When selecting any pyrometer for operation within an industrial setting a few issues have to be addressed. Gases, fumes, sparks and plasmas may disturb the measurement in a number of ways. The viewing angle and optics should be chosen so that the effect of such disturbances along with reflections are minimised. The wavelength at which the pyrometer measures should ideally be chosen so that absorption in gases and fumes are minimised. Also it should be selected so that it does not coincide with possible emission lines from plasmas or other excited species. Furthermore the selected wavelength should be appropriate for the temperature range in interest, a subject further elaborated on in Section 5.3.

The effect of surface oxidation of steels has been described by Bauer et al. [19] and Thiessen et al. [20] to affect temperature measurements. This most probably also affects titanium alloys in general, including Ti–6Al–4V, since they easily form surface oxide layers [21]. This leads to the conclusion that surface oxidation behaviour during heat processing is an important issue in temperature measurements.

2.3. Methods for emissivity measurements

There are a number of alternatives for finding the emissivity of a material including theoretical studies based on knowledge of refractive indices [22,23], reflectance measurements at normal incidence angles [24], multispectral methods [25] and sample levitation methods [26]. None of these methods are applicable in an industrial setting for different reasons, namely refractive indices vary with temperature [27], in site reflectance measurements are not viable for varying angles of incidence and there is in general no reliable model for spectral emissivity available.

2.4. Emissivity of Ti–6Al–4V

Data collected by Milošević and Maglić [28] shows that the estimation of hemispherical total emissivity of pure titanium for temperatures between 1000 K and 1950 K vary very much between measurements. Even if separate papers [28,26] report linear correlation between temperature and hemispherical total emissivity, differences between highest and lowest reported emissivity values are as large as 0.1. A spectral radiation pyrometer is dependent on the directional spectral emissivity, which is a constituent of the hemispherical total emissivity. One could suspect that variations in directional spectral emissivity would be present and affect measurements if the total hemispherical emissivity varies during similar conditions.

Since surface properties greatly affect emissivity, the discrepancies between measurements can be attributed to varying surface conditions [13]. As pure titanium exhibits this varying emissivity between measurement procedures, it is assumed that the alloy investigated shows similar behaviour, since it is dominated by titanium. There are however good reasons not to assume that the emissivity characteristics of Ti–6Al–4V is equal to that of pure titanium. Among those are the findings of Shur and Peletskii

[29] showing that alloying elements affect emissivity for titanium alloys.

The alloy used is also subject to elemental segregation when heated [30,21]. This causes adsorbate elements migrate into the bulk if Ti–6Al–4V is heat processed such as in LMD. Since titanium surfaces are oxidised if ever subjected to oxygen [21], the migration of oxygen and other adsorbate elements also affect emissivity when the sample is heated. Titanium dioxide shows phase transitions between anatase and rutile in the temperature region of interest [31]. The oxide layer is therefore assumed to have varying emissivity characteristics during a heat processing cycle typical for LMD. Time–temperature history plays a vital role in oxide growth and migration [30]. The surface emissivity is affected through a varying oxide layer thickness and is therefore also an integral over time–temperature history. It would require argon sputtering, long time heating in totally oxygen-free atmosphere or some other cleaning method in order to have a non-contaminated Ti–6Al–4V surface [30].

2.5. Reference paints

As described by Brandt et al. [32] there exist emissivity reference paints with specified emissivity suitable for high temperature applications. Such paints could be applied in areas of a body which are interesting to monitor by radiation pyrometry. However the temperature in these areas must not exceed the highest specified temperature limit of the paint. Such paint could also be employed with radiation pyrometers as an emissivity reference during calibration as it is used in this study.

3. Method for emissivity estimation

The argumentation by Zhang and Machin [2] favoured a narrow wavelength radiation pyrometer if no reliable model of the spectral emissivity is available. One of the reasons for using such pyrometer in the current study is the lack of sufficient knowledge to model spectral emissivity.

In a study [29], Shur and Peletskii investigated the temperature varying emissivity behaviour for Ti–6Al–4V. It was performed in oil-less vacuum and estimated total hemispherical emissivity, which is not equal to spectral emissivity used in a narrow waveband pyrometer. The results in that study are therefore not applicable to measurements in the LMD process where oxidation occurs.

The requirement of argon sputtering, long time heating in totally oxygen-free atmosphere in order to have a non-contaminated Ti–6Al–4V surface is questionable in industrial use and is not viable for the LMD process. From these facts it was concluded that emissivity estimation should be performed in process conditions resembling industrial conditions.

The emissivity estimation proceeds as follows. A signal $u(T_R,\varepsilon)$ from a virtual pyrometer measuring the reference temperature T_R and with a correct emissivity setting $\varepsilon(\lambda,T_R)$ is set equal to the signal from the physical radiation pyrometer $u_r(T_P,\varepsilon_p)$ with a centre wavelength λ_c and which is measuring the temperature T_P at the measurement spot with temperature T_R:

$$u_r(T_P,\varepsilon_p) = u(T_R,\varepsilon). \tag{7}$$

If the emissivity setting of the radiation pyrometer, ε_p, is known, the following relation is applicable:

$$\frac{\kappa\varepsilon_p 2\pi C_1\Delta\lambda}{\lambda_c^5(e^{C_2/(\lambda_c T_P)}-1)} = \frac{\kappa\varepsilon(\lambda_c,T_R)2\pi C_1\Delta\lambda}{\lambda_c^5(e^{C_2/(\lambda_c T_R)}-1)}. \tag{8}$$

Using (8), one can readily deduce the following relation:

$$\varepsilon(\lambda_c,T_R) = \varepsilon_p\frac{e^{C_2/(\lambda_c T_R)}-1}{e^{C_2/(\lambda_c T_P)}-1}. \tag{9}$$

Here the centre wavelength λ_c is used in the modelling. There are more accurate ways to model the wavelength dependency e.g. to calculate a so called mean effective wavelength, see e.g. the suggestions by Saunders [33]. However, the importance of an accurate calculation of the mean effective wavelength is more prominent when considering a wider measuring wavelength region than the one considered here. Eq. (9) can be used for estimating emissivity based on the pyrometer emissivity setting ε_p, measured temperature T_P and a temperature reference T_R.

4. Experimental procedure

A number of experiments have been performed with the two most significant listed in Table 1. A narrow waveband radiation pyrometer (Impac IGA 5-LO MB25, λ_r = 1.45, . . ., 1.8 μm) has been used for measuring on an induction heated metal specimen. The metal was in the form of a solid Ti–6Al–4V boss deposited with LMD on a base plate of the same material, see Fig. 1. This radiation pyrometer measurement has then been compared with measurements from either a pyrometer measurement on the boss in a neighbouring area with emissivity reference paint or measurements from a neighbouring thermocouple.

It is assumed that the temperature distribution was homogeneous in the measurement area of the boss since it is a symmetric geometry, there was no forced convection in the surrounding atmosphere, and it displayed a homogeneous colour during heating above the glowing temperature.

The temperature range of the measurand during the experiments was 750 K to at least 1330 K whereas the ambient was held at room temperature. Thus there was no significant irradiation from ambient atmosphere during measurement. Due to the reactivity of the Ti–6Al–4V with oxygen, the thermal cycling was carried out in an argon filled chamber with an oxygen level typically below 10 ppm. During the experiments the oxygen level was monitored with a PBI Dansensor SGI-3.

Table 1
Trial parameters.

	Trial 1	Trial 2
Thermocouple type	S&N	K
Reference paint	HE23 [32]	–
Robot reorientation	Y	N
Measured O_2-level	1 ppm	<1 ppm
Maximum temperature	1550 K	1330 K
Steel wool for O_2-trapping	N	Y

The induction heater was used in closed loop with the thermocouple signal in order to control the heating. The temperature signal was fed to a proportional–integral–derivative (PID) controller, which controlled the current through the induction coil. During the experiments the temperature was stepwise increased between several stationary levels and also continuously either increased or decreased between different levels. A computer program implemented in the LabVIEW software, collected measurement data, communicated with the robot system and was used to implement the controller.

In all trials the radiation pyrometer was at an angle of ($\theta = 25^{\circ}$) from the surface normal, an angle typical for LMD and sufficiently small in order to neglect the angle dependency [13]. The pyrometer signal, u_r, was recorded through the pyrometer's 4–20 mA analog output and the emissivity parameter ε_p was manually set at 100%.

In **Trial 1** an industrial robot IRB 1400 from ABB Robotics was used to reorient the pyrometer's measurement spot between the reference painted area and an neighbouring area of bare metal. The paint was obtained by courtesy of Rolls-Royce [32]. The temperature values obtained from the radiation pyrometer when pointed at the paint were complemented with simultaneous thermocouple readings. In order to have good temperature references in **Trial 1**, two independent thermocouples of type N and S were mounted on the boss surface.

To facilitate a reduction of the oxygen level in the gas chamber in **Trial 2**, steel wool was heated through a high current system which caused the steel wool to glow. This increased the chemical reactivity of the iron, effectively making it an oxygen trap. This was confirmed by visual inspection of the steel wool which blackened after heating. Separate trials showed decreasing oxygen levels when the steel was heated and an increasing O_2-level when the heating was turned off. In **Trial 2** a thermocouple of type K was used.

5. Calibration results and discussion

From preliminary tests it was discovered that type N thermocouples were seriously affected by the heat. Therefore both type N and S thermocouples were employed for **Trial 1** where a temperature of 1623 K was reached. This high temperature was recorded with type S thermocouples whilst the type N never gave higher readings than 1550 K. The type N thermocouples used for the experiments are Inconel sheathed. Inconel has nickel as main constituent [34]. From the binary phase diagram for Ni–Ti it is obvious that the alloys formed has a significantly lower melting temperature than that of the pure elements for certain ratios [35]. Such a ratio is found in the phase diagram around 65 weight percent nickel where there is an eutectic point with a temperature that corresponds well to our measured value 1550 K. This is a drastic reduction of the melting temperature compared to 1900 K which is the approximate melting point for Ti–6Al–4V [36,37]. For the ternary system Al–Ni–Ti, a similar trend can be seen for low aluminium content [38]. On the basis of this, it is reasonable to assume that a diffusion driven alloying process causes formation of a phase with lower melting temperature. This explains the melting and cavities found in the Ti–6Al–4V test piece.

5.1. Implications on Trial 1

The aforementioned observations resulted in using type S platinum based thermocouples as well as type N thermocouples in **Trial 1**. The type S thermocouples proved more robust but nevertheless showed a similar behaviour at temperatures above 1723 K where they fused with the titanium alloy and melted as shown in Fig. 1. This behaviour can be traced back to the binary phase diagram for titanium and platinum, which are the dominating elements in the materials [39].

Also the reference paint was affected by the heat in **Trial 1** in a way not anticipated. At 1473 K the radiation pyrometer signal dropped significantly and smoke arose from the boss. After examination it was clear that the paint had evaporated or diffused into the bulk. This is in disagreement with claims put forward by Brandt et al. [32].

5.2. Uncertainty in emissivity and temperature

The uncertainty in temperature estimation using (9) is assumed to depend partly upon measurement uncertainties and partly due to the fact that the estimated emissivity during LMD processing could differ from the estimated emissivity used in calibration of the pyrometer. This difference is the result of time–temperature history of the surface oxidation in each separate case.

5.2.1. Measurement uncertainty

The estimation of measurement uncertainty is made in accordance with *Guidelines for evaluating and expressing the uncertainty of NIST measurement results* [40]. In order to establish the uncertainty in the emissivity estimate (9) the uncertainties of the independent variables T_P and T_R have to be known. These temperature uncertainties are type B evaluations from manufacturer's specifications. It

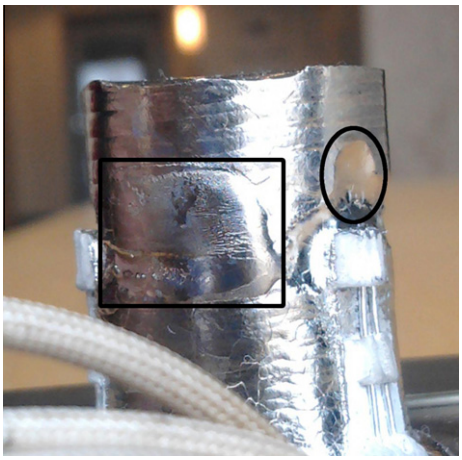

Fig. 1. Paint after heating above 1473 K in rectangle. In the ellipse: the molten type S thermocouple.

can be assumed that these specifications are statements of the limits of the error and that all values of the error within these limits are equally probable (rectangular distribution). The contribution of standard uncertainty in each case is therefore the limits of error divided by $\sqrt{3}$ [40].

The estimate (9) is calculated as a function of T_R and T_P when the radiation pyrometer setting for ε_p is unity and the wavelength λ_c is regarded constant. Introduce the function;

$$f(T_P, T_R) = \frac{e^{C_2/(\lambda_c T_R)} - 1}{e^{C_2/(\lambda_c T_P)} - 1}. \tag{10}$$

The uncertainty in (10) is a combined uncertainty $\Delta\varepsilon_{c_1}$ calculated as;

$$\Delta\varepsilon_{c_1} \approx \sqrt{\left(\frac{\partial f}{\partial T_P}\right)^2 \Delta T_P^2 + \left(\frac{\partial f}{\partial T_R}\right)^2 \Delta T_R^2}. \tag{11}$$

A comparison of the sensitivity coefficients $\frac{\partial f}{\partial T_P}$ and $\frac{\partial f}{\partial T_R}$ in the relevant temperature region shows that they are very close in magnitude meaning that there is no reason to specify different demands on measurement accuracy for T_P or T_R.

5.2.2. Emissivity variations due to time–temperature history

In addition to the measurement uncertainties described above, uncertainty in emissivity estimations also comprises an uncertainty in the instant surface emissivity $\Delta\varepsilon_{c_2}$ causing a hysteresis. The origin of this uncertainty is the variable oxidation level of a Ti–6Al–4V-surface due to the time–temperature history. The magnitude of these emissivity variations, $\Delta\varepsilon_{c_2}$, is estimated from experimental data by using the maximum deviations in emissivity estimates. The combined standard uncertainty is thus the sum of $\Delta\varepsilon_c = \Delta\varepsilon_{c_1} + \Delta\varepsilon_{c_2}$.

The expanded uncertainty $\Delta\varepsilon = 2\Delta\varepsilon_c$ is based on the combined standard uncertainty multiplied by a coverage factor of 2, which provide a confidence level of approximately 95% [40].

5.3. Resulting uncertainty in temperature measurement

The partial derivatives of the expression for the radiance of a physical body, i.e. $i_p = \varepsilon i_b$ with respect to the emissivity ε and temperature (here is T_P used), is employed in the derivation of the expression for how the relative uncertainty in emissivity propagates to a relative uncertainty in temperature;

$$\frac{\Delta T_P}{T_P} \approx \frac{T_P \lambda_c}{C_2}\left(1 - e^{-\frac{C_2}{T_P \lambda_c}}\right)\frac{\Delta\varepsilon}{\varepsilon}. \tag{12}$$

From (12) it is readily seen that the relative uncertainty of the temperature can be minimised by choosing a short measuring wavelength λ_c. However, this choice is usually a trade off between the wavelength region of the pyrometer and the desired temperature region to be measured. A shorter wavelength generally results in a temperature range of higher temperatures. The choice of measuring wavelength is here also constrained by the wavelength of the laser source used in the LMD process. It is not recommendable to measure at the same wavelength as this high power source.

The specified limits of error for the radiation pyrometer is ±0.3% of the reading ±1 K [41], the specification for the thermocouples is ±0.25% of the reading [42]. The specification for the analogue input module used for the radiation pyrometer is a combined gain and offset error less than ±2 K [43], and the specification for the thermocouple input device is less than ±4 K [44]. From this information the standard uncertainty ΔT_R for the thermocouple measurements never exceeded ±4 K and the standard uncertainty ΔT_P from radiation pyrometer measurements never exceeded ±3 K.

The relative uncertainty in temperature in the range between 750 K and 1550 K never exceeded 2.5 % in any experimental trial. This is considered sufficient for the intended purposes of on-line control and calibration of process models. This can be compared to a typical uncertainty of a thermocouple measurement of approximately 0.5%. Due to the hysteresis behaviour in emissivity, a more accurate estimation cannot be concluded from the current experiment. As the hysteresis was repeatable over multiple temperature sweeps it cannot be regarded as measurement error.

5.4. Phase transitions

Fig. 2 shows measured emissivity together with upper and lower (95 %) confidence interval as functions of temperature for **Trial 1** calculated from (11). A significant hysteresis was present where the emissivity was dependent on whether the material has been heated or cooled. The higher values were reached when heating the boss and the result was repeatable over several temperature cycles. The hysteresis was caused by oxidation and metal phase transformations.

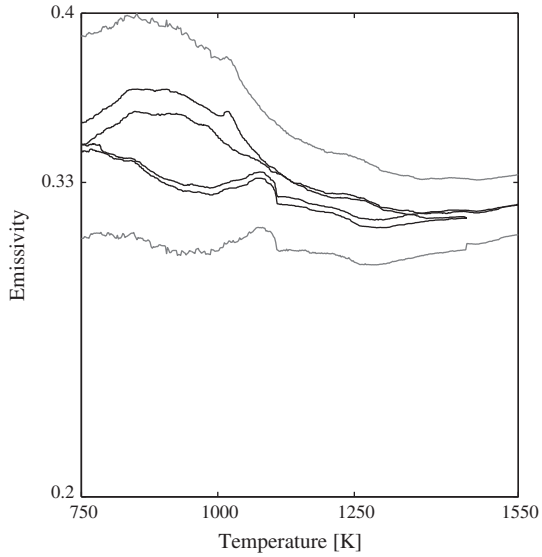

Fig. 2. Emissivity estimate from **Trial 1** exhibiting hysteresis. Upper and lower boundaries of estimation are indicated with grey lines.

During cooling Ti–6Al–4V exhibits a transformation between β and α phases in the temperature span from 1123 K to 1023 K [45,46]. Due to the energy exerted by the transformation, a non-linearity in temperature–time dependence was present during the cooling phase. As only heat input was controlled, a slow but substantial release of latent heat caused the control signal (the current in the induction coil) to reach its lower limit during cooling and the temperature to deviate from the target temperatures. In Fig. 2, the range between 1010 K and 1110 K exhibit "lumps" in the emissivity curve, which was most probably caused by said phase transitions.

5.5. Modelling of emissivity behaviour

The emitting surface was regarded as an opaque metallic base material with a thin oxide layer on top. For titanium and titanium alloys it is well established that visible changes in perceived colouring of the material is directly related to the thickness of the oxide layer [47,48]. Since no colour change was visible for the treated specimen shown in Fig. 1 it is assumed that the oxide layer thickness is below 100 nm. This in turn leads to the assumption that said oxide layer is transparent for the measured wavelength since its thickness is well below a quarter wavelength and even an eighth of the employed wavelength. Interference effects should be negligible for such thin layers. For thin films with thicknesses that are below a quarter of the wavelength a linear approximation of the emissivity contribution of the film is reasonable [22,23].

Hence, an additive model was assumed where the surface emissivity consists of additive terms from the metal and the oxide layer described as:

$$\varepsilon = \varepsilon_m + \varepsilon_o = \varepsilon_m + k_1 d. \tag{13}$$

The oxide layer thickness, d, is assumed to grow at a rate independent of temperature but dependent on the probability of an O_2-molecule adsorbing to the surface. The oxide layer height d is normalised in order to also describe the fractional availability of oxidation sites on the surface which is assumed to be proportional to layer height. The probability of oxygen sticking to the surface, P, was modelled as $P = p_{O_2}(1-d)$ where $0 \leqslant d \leqslant 1$ and p_{O_2} is the partial pressure of oxygen in the gas chamber [49]. Above an activation temperature, T_{act} ($\approx$810 K for pure Ti), the oxide diffuses into the bulk material and d is decreased [21,30]. This results in the non-linear system model described as;

$$\dot{d} = k_2 p_{O_2}(1-d) - k_3 d(T - T_{act})H(T - T_{act}), \tag{14}$$

where $H(x)$ is the Heaviside step function and

$$\varepsilon = \varepsilon_m + k_1 d. \tag{15}$$

When tuning initial oxide thickness d_0 along with the other model parameters, the typical features for the measured emissivity hysteresis curve are captured as shown in Fig. 3. It should be noted that the model is only proposed for the elevated temperatures examined. As temperatures decrease, the diffusivity of the oxide layer and the number of available sites decrease.

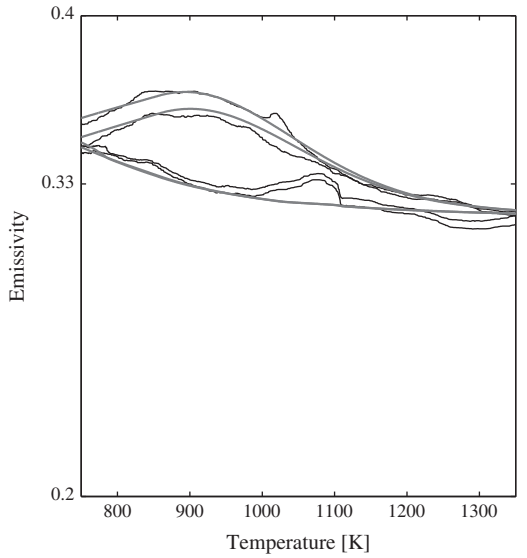

Fig. 3. Estimated (black line) and modelled (grey line) emissivity.

The inability to describe all features in the emissivity characteristics is due to the lack of phase transition modelling within the proposed model. As mentioned above, both Ti–6Al–4V and TiO_2 exhibit phase transitions in the examined temperature range. Due to these effects and the fact that the initial oxidation state of the surface is unknown, the proposed model should not be used for predicting emissivity but rather be seen as a possible explanation of the observed emissivity characteristic.

Assuming that a melted bead of Ti–6Al–4V is not initially oxidised, it is only necessary to establish the rate of oxide growth or change of oxide layer thickness during processing in order to correctly estimate the oxide's effect on surface emissivity since d_0 is zero. However this might prove difficult for practical reasons. What is a suitable temperature reference for measuring a rapidly cooling melt? How does one ensure constant processing conditions with respect to oxygen content since the processing itself will alter the oxygen level in the processing atmosphere?

Monitoring oxygen levels and using this information in order to calculate the emissivity at each instance of time is limited by the accuracy of the model used. The formulation and calibration of such an elaborate model is a very time consuming task which may end up not to capture all relevant parameters due to the complex processes modelled. In the case of using a model for calculating emissivity without a reference, temperature would also be an input to the model which makes the calculation recursive and sensitive to accumulated errors. Instead one could resort to *in situ* emissivity measurement methods such as ellipsometry or reflectivity measurements. These methods are complicated and are not well suited for use in for example robotised LMD [2]. Also the impact of titanium oxide introduced through the use of a wire would have to be investigated *a priori*.

The possible improvements presented above might not prove to be worth the effort since the accuracy of the temperature measurements is not the only factor determining the quality of simulations [8,7]. For control purposes, absolute temperature measurements are not always necessary and the actuating side of the control system might be the limiting factor for good process control [1,50].

5.6. Implications on Trial 2

The knowledge gained from **Trial 1** and the proposed oxidation model enabled calibration for the LMD-process through an additional trial. It is assumed that the oxide layer of a newly deposited bead is best approximated with unoxidised metal due to the rapid cooling rate. The rapid cooling disallows extensive oxidation since the material quickly cools down enough to substantially lower the reactivity of the surface with O_2. In order to simulate the rapid cooling of a deposited bead without initial oxidation it is necessary to minimise the oxygen content during the much longer time periods of elevated temperature affecting the induction heated Ti–6Al–4V boss. Minimisation of the O_2 level was accomplished using heated steel wool. However a noticeable effect of oxidation is still seen. The aim of this trial was not to measure high temperatures but to keep a low oxygen level. Therefore an Ni-based thermocouple of type K was used. First the boss was heated to approximately 850 K in approximately 3 min in order to reduce surface oxidation [30,21]. After heating, the boss was allowed to cool down to 673 K. During cooling in approximately 160 s there was a noticeable change in the emissivity level. However, this level was roughly constant during the rest of the experiment. The thermocouple alloyed with the base material at 1330 K during this trial which is consistent with the Ni–Ti phase diagram [35]. The result from **Trial 2**, presented in Fig. 4, is believed to more accurately than the results from **Trial 1** describe

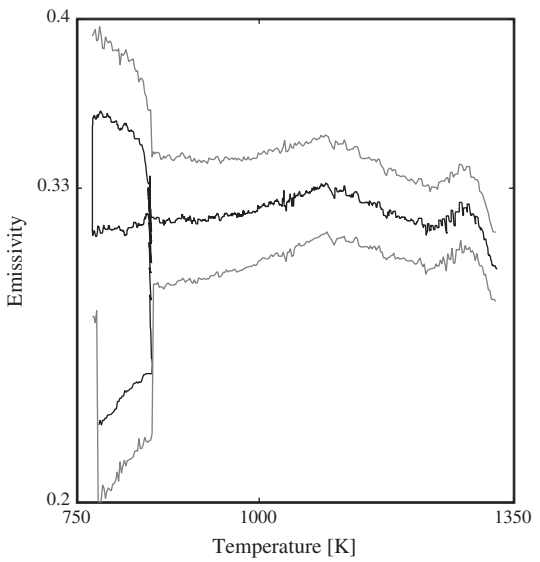

Fig. 4. Emissivity estimate from **Trial 2**.

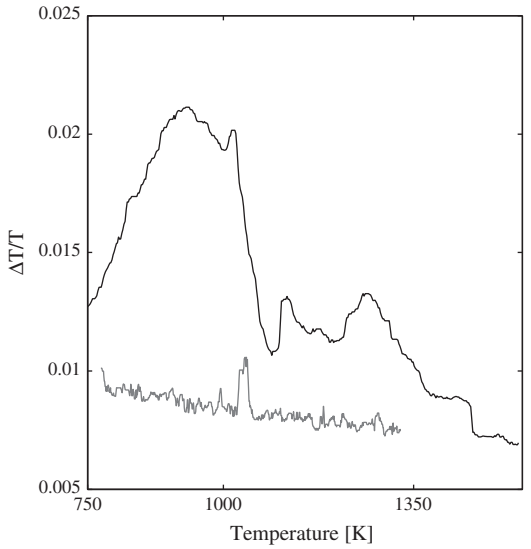

Fig. 5. Relative temperature error when using a calibrated radiation pyrometer. Higher values resulted from **Trial 1** and lower values from **Trial 2**.

the properties for unoxidised Ti–6Al–4V since the oxidation is kept at a minimum. It is apparent in Fig. 5 that the temperature errors are lower when the oxide layer does not vary as much as in **Trial 1**.

6. Conclusions

It has been shown that a narrow wavelength radiation pyrometer can be calibrated with type S thermocouples for temperature measurements of Ti–6Al–4V up to 1550 K using the proposed strategy. The resulting temperature uncertainty is less than 2.5%, which is considered as sufficient, especially when regarding the low value of emissivity of shiny Ti–6Al–4V.

A heat resistant reference paint with specified emissivity was evaluated but found not to be sufficiently resistant for the application since the it evaporated or diffused at temperatures above 1473 K.

Temperature measurements of Ti–6Al–4V proved not to be compatible with type S thermocouples above 1723 K, with type N thermocouples above 1553 K or with type K thermocouples above 1330 K.

When applied to LMD, a calibrated narrow wavelength radiation pyrometer proved to be useful for measuring high temperatures during processing. Minimising the oxygen content in the chamber while performing calibration will allow oxidation rates that are well suited for mimicking the rapid temperature changes present in LMD. This is possible while still performing calibration using thermocouples and controlled heating, a procedure which is significantly slower than weld bead cooling and heating in LMD. However, as material oxidation characteristics vary with process environment and as emissivity changes with heating and cooling, measurements with higher accuracy will require *in situ* emissivity characterisation.

The proposed procedure is valid for the specified measurement situation with the evaluated pyrometer and material and atmosphere typical for the LMD process. However, due to the simplicity of the procedure, other radiation pyrometers, metals and heating processes can be investigated in a similar fashion.

Acknowledgements

The authors wish to acknowledge the contributions from: Hans Dahlin (induction heater and oxygen trap), Almir Heralić (LMD know-how and Ti–6Al–4V-material), Volvo Aero Company (financial support via the NFFP-project MD-Reg and supply of thermocouples), Rolls Royce Germany (emissivity reference paint). The research leading to these results has received funding from the European Communitys Seventh framework Programme FP7 2007–2013 under Grant Agreement 266271 – Merlin Project.

References

[1] A. Heralic, Monitoring and control of robotized laser Metal–Wire deposition, Doctoral thesis, Chalmers University of Technology, 2012.
[2] Z.M. Zhang, B.K. Tsai, G. Machin, Radiometric Temperature Measurements, Fundamentals, vol. 42: I, Academic Press, 2009.
[3] D.P. DeWitt, G.D. Nutter, Theory and Practice of Radiation Thermometry, Wiley IEEE, 1988.
[4] Z.M. Zhang, B.K. Tsai, G. Machin (Eds.), Radiometric temperature measurements, in: Applications, vol. 43: II, first ed., Academic Press, 2009.
[5] J. Destefani, Introduction to titanium and titanium alloys, in: Properties and Selection: Nonferrous Alloys and Special-Purpose Materials, Vol. 2, ASM Handbook, ASM International, 1990, pp. 586–591.
[6] A. Lundbäck, Modelling and simulation of welding and metal deposition, Doctoral thesis, Luleå University of Technology, Luleå, 2010.
[7] Corinne Charles, Niklas Järvstråt, Modelling Ti–6Al–4V microstructure by evolution laws implemented as finite element subroutines: Application to TIG metal deposition, in: Trends in Welding Research: Proceedings of the 8th International Conference, June 1–6, 2008, Callaway Gardens Resort, Pine Mountain, Georgia, USA, 2009, pp. 477–485.
[8] M. Edstorp, Numerical simulation of heat transfer and fluid flow during laser metal wire deposition, in: 2011 ICALEO Congress Proceedings, Laser Institute of America, Orlando, FL, USA, 2011.
[9] G. Bi, A. Gasser, K. Wissenbach, A. Drenker, R. Poprawe, Identification and qualification of temperature signal for monitoring and control in laser cladding, Optics and Lasers in Engineering 44 (12) (2006) 1348–1359.
[10] M. Doubenskaia, P. Bertrand, I. Smurov, Optical monitoring of Nd: YAG laser cladding, Thin Solid Films 453 (2004) 477–485.
[11] E. Toyserkani, A. Khajepour, S. Corbin, Laser Cladding, CRC Press, 2005.
[12] M. Planck, The Theory of Heat Radiation, P. Blakiston's Son & Co., 1906.
[13] R. Siegel, J.R. Howell, Thermal Radiation Heat Transfer, Taylor & Francis, 2002.
[14] L. del Campo, R.B. Pérez-Sáez, L. González-Fernández, X. Esquisabel, I. Fernández, P. González-Martín, M.J. Tello, Emissivity measurements on aeronautical alloys, Journal of Alloys and Compounds 489 (2) (2010) 482–487.
[15] R. Felice, Pyrometry for liquid metals, Advanced Materials & Processes (2008) 31.
[16] T. Duvaut, D. Georgeault, J.L. Beaudoin, Multiwavelength infrared pyrometry: optimization and computer simulations, Infrared Physics & Technology 36 (7) (1995) 1089–1103.
[17] T. Duvaut, Comparison between multiwavelength infrared and visible pyrometry: application to metals, Infrared Physics & Technology 51 (4) (2008) 292–299.
[18] P.B. Coates, Multi-wavelength pyrometry, Metrologia 17 (3) (1981) 103–109.
[19] W. Bauer, A. Moldenhauer, F. Rogge, Influence of a growing oxide layer on band-emissivities used for optical temperature measurements, in: Proceedings of SPIE, vol. 7299, Orlando, FL, USA, 2009, pp. 1–8.
[20] R.G. Thiessen, E. Bocharova, D. Mattissen, R. Sebald, Temperature measurement deviation during annealing of multiphase steels, Metallurgical and Materials Transactions B 41 (4) (2010) 857–863.
[21] Y. Mizuno, F.K. King, Y. Yamauchi, T. Homma, A. Tanaka, Y. Takakuwa, T. Momose, Temperature dependence of oxide decomposition on titanium surfaces in ultrahigh vacuum, Journal of Vacuum Science & Technology A: Vacuum, Surfaces, and Films 20 (2002) 1716.
[22] P. Pigeat, D. Rouxel, B. Weber, Calculation of thermal emissivity for thin films by a direct method, Physical Review B 57 (15) (1998) 9293–9300.
[23] T. Iuchi, T. Furukawa, S. Wada, Emissivity modeling of metals during the growth of oxide film and comparison of the model with experimental results, Applied Optics 42 (13) (2003) 2317–2326.
[24] R.R. Corwin, A. Rodenburgh II, Temperature error in radiation thermometry caused by emissivity and reflectance measurement error, Applied Optics 33 (10) (1994) 1950–1957.
[25] A. Magunov, Spectral pyrometry (review), Instruments and Experimental Techniques 52 (4) (2009) 451–472.
[26] P. Paradis, W. Rhim, Non-contact measurements of thermophysical properties of titanium at high temperature, The Journal of Chemical Thermodynamics 32 (1) (2000) 123–133.
[27] G.M.W. Kroesen, G.S. Oehrlein, T.D. Bestwick, Nonintrusive wafer temperature measurement using in situ ellipsometry, Journal of Applied Physics 69 (5) (1991) 3390–3392.
[28] N.D. Milošević, K.D. Maglić, Thermophysical properties of solid phase titanium in a wide temperature range, High Temperatures – High Pressures 37 (2008) 184–204.
[29] B.A. Shur, V.E. Peletskii, The effect of alloying additions on the emissivity of titanium in the neighborhood of polymorphous transformation, High Temperature 42 (3) (2004) 414–420.
[30] M.S. Dhlamini, H.C. Swart, J.J. Terblans, C.J. Terblanche, Surface cleaning of a commercially pure ti, Ti6Al4V and Ti3Al8V6Cr4Zr4Mo alloys by linear heating, Surface and Interface Analysis 38 (4) (2006) 339–342.
[31] D.J. Won, C.H. Wang, H.K. Jang, D.J. Choi, Effects of thermally induced anatase-to-rutile phase transition in MOCVD-grown TiO2 films on structural and optical properties, Applied Physics A: Materials Science & Processing 73 (5) (2001) 595–600.
[32] R. Brandt, C. Bird, G. Neuer, Emissivity reference paints for high temperature applications, Measurement 41 (7) (2008) 731–736.
[33] P. Saunders, General interpolation equations for the calibration of radiation thermometers, Metrologia 34 (3) (1997) 201–210.
[34] R. Steiner, ASM Handbook Volume 1: Properties and Selection: Irons, Steels, and High-Performance Alloys, 10th ed., ASM International, 1990.
[35] ASM, ASM Handbook: Volume 3: Alloy Phase Diagrams (ASM Handbook), 10th ed., ASM International, 1992.
[36] J.R. Davis, A.I.H. Committee, Metals Handbook Desk Edition, second ed., CRC Press, 1998.
[37] M. Boivineau, C. Cagran, D. Doytier, V. Eyraud, M.H. Nadal, B. Wilthan, G. Pottlacher, Thermophysical properties of solid and liquid Ti–6Al–4V (TA6V) alloy, International Journal of Thermophysics 27 (2) (2006) 507–529.
[38] K. Zeng, R. Schmid-Fetzer, B. Huneau, P. Rogl, J. Bauer, The ternary system Al–Ni–Ti part II: thermodynamic assessment and experimental investigation of polythermal phase equilibria, Intermetallics 7 (12) (1999) 1347–1359.
[39] H. Okamoto, Pt–Ti (platinum–titanium), Journal of Phase Equilibria and Diffusion 30 (2) (2009) 217–218.
[40] B. Taylor, C. Kuyatt, Guidelines for evaluating and expressing the uncertainty of NIST measurement results, National Institute of Standards and Technology Gaithersburg, MD, US, 1994.
[41] Impac, IGA 5-LO user manual, User manual, Impac, 2011.
[42] IEC, IEC 60584-2, amendment 1 – thermocouples. Part 2: Tolerances, IEC Standard, International Electrotechnical Commision, June 1989.
[43] National Instruments, NI 9203, Data sheet, National Instruments, 2011.
[44] National Instruments, NI 9211, Data sheet, National Instruments, 2011.
[45] R. Pederson, The microstructures of Ti–6Al–4V and Ti–6Al–2Sn–4Zr–6Mo and their relationship to processing and properties, Doctoral thesis, Luleå University of Technology, Luleå, June 2004.
[46] S. Malinov, P. Markovsky, W. Sha, Z. Guo, Resistivity study and computer modelling of the isothermal transformation kinetics of

Ti–6Al–4V and Ti–6Al–2Sn–4Zr–2Mo–0.08Si alloys, Journal of Alloys and Compounds 314 (1–2) (2001) 181–192.
[47] A. Pérez del Pino, J. Fernández-Pradas, P. Serra, J. Morenza, Coloring of titanium through laser oxidation: comparative study with anodizing, Surface and Coatings Technology 187 (1) (2004) 106–112.
[48] M.V. Diamanti, B. Del Curto, M. Pedeferri, Interference colors of thin oxide layers on titanium, Color Research & Application 33 (3) (2008) 221–228.
[49] G. Attard, C. Barnes, Surfaces, Oxford University Press, 1998.
[50] F. Sikström, Modeling and simulation for welding automation, Ph.D thesis, Chalmers University of Technology, 2010.